Probing domain microstructure in ferroelectric $Bi_4Ti_3O_{12}$ thin films by optical second harmonic generation

Yaniv Barad, James Lettieri, Chris D. Theis, Darrell G. Schlom, and Venkatraman Gopalan[a)]
Material Research Laboratory and Department of Materials Science and Engineering, Pennsylvania State University, University Park, Pennsylvania 16801

J. C. Jiang and X. Q. Pan
Department of Materials Science and Engineering, The University of Michigan, Ann Arbor, Michigan 48109

(Received 5 September 2000; accepted for publication 29 October 2000)

The domain microstructure in an epitaxial thin film of $Bi_4Ti_3O_{12}$ on a $SrTiO_3(001)$ substrate is studied by second harmonic generation measurements. The input polarization dependence of the second harmonic signal exhibits spatial symmetries that reflect the presence of eight different domain variants present in the film. A theoretical model is presented that explains the observed symmetries and extracts quantitative information on the nonlinear optical coefficients of the material and statistics of domain variants present in the film area being probed. The following ratios of nonlinear coefficients and birefringence was determined: $d_{12}/d_{11}=-3.498\pm0.171$, $|d_{26}/d_{12}|=0.365\pm0.010$, $|d_{26}/d_{11}|=1.273\pm0.036$, and $|n_b-n_a|=0.101\pm0.018$ (at 532 nm). © *2001 American Institute of Physics.* [DOI: 10.1063/1.1334641]

I. INTRODUCTION

Aurivillius phases are of interest in nonvolatile memory since several of them exhibit excellent fatigue resistance during repeated polarization reversals with electric field.[1] Bismuth titanate, $Bi_4Ti_3O_{12}$, is an important member of the highly layered aurivillius phase perovskite oxides of the type $(Bi_2O_2)^{2+}(Me_{x-1}R_xO_{3x+1})^{2-}$ where Me is a monovalent or a divalent element such as Bi^{2+}, Ba^{2+}, Sr^{2+}, K^{1+}, Ca^{2+}, Na^{+}, Pb^{2+}, and several rare earth ions, R may be Ti^{4+}, Nb^{5+}, Ta^{5+}, Mo^{6+}, W^{6+}, Ga^{3+}, Fe^{3+}, Cr^{3+}, and x can be 1 to 8.[2] Epitaxial growth of $Bi_4Ti_3O_{12}$ films on various substrates invariably results in a complex domain microstructure, resulting from the fact that the spontaneous polarization in a monoclinic unit of $Bi_4Ti_3O_{12}$ has components along both the a- and c- crystallographic directions where $a-c$ forms the mirror plane (010). Both a and c components of the polarization can be independently reversed, thus resulting in four different classes of domain walls and 18 wall configurations.[3] All these configurations are not readily distinguishable by conventional x-ray diffraction or transmission electron microscopy (TEM). In this article, we show how probing the second harmonic generation (SHG) response of a $Bi_4Ti_3O_{12}$ film with a complex domain microstructure can provide many of these domain distinctions in a quantitative manner.

II. FILM EPITAXY AND DOMAIN MICROSTRUCTURE

The $Bi_4Ti_3O_{12}$ thin film studied here was grown on a $SrTiO_3(001)$ substrate using molecular-beam epitaxy as previously reported in detail.[4] The lattice parameters of the cubic $SrTiO_3(001)$ substrate, $a'=3.9050$ Å closely match along its diagonals of $a'\sqrt{2}$, with the lattice parameters $a=5.4500$ Å and $b=5.4059$ Å of the monoclinic $Bi_4Ti_3O_{12}$. (The other lattice parameters are $c=32.832$ Å, and $\beta=90.00°$).[5] The lattice planes $b-c$, $c-a$, and $a-b$ of $Bi_4Ti_3O_{12}$ are respectively denoted as (100), (010), and the (001) planes. The θ–2θ and ϕ-scan x-ray diffraction spectra of the film shown in Fig. 1, indicate that the $Bi_4Ti_3O_{12}$ film has grown epitaxially on the underlying $SrTiO_3$ substrate. The epitaxial orientation relationship is $SrTiO_3(001)[110]//Bi_4Ti_3O_{12}(001)[100]$. In this configuration, there are eight possible domain configurations of the $Bi_4Ti_3O_{12}$ as shown schematically in Fig. 2. Each of the possible domains has a monoclinic unit cell, which deviates only slightly from the orthorhombic unit cell. The polarization axis forms an angle of ~4.5° from the crystallographic a axis in the $a-c(010)$ plane.

Figure 3 shows the various domain walls that can arise from a combination of these domain variants. In particular, referring to the pseudo-orthorhombic planes of $Bi_4Ti_3O_{12}$, four main types of domain walls can exist: (I) Nearly-90° domain walls along the (110) planes, (II) domain walls separating variants with opposite a component of polarization. These walls are either neutral (001) planes or charged (100) planes. (III) domain walls separating variants with opposite c component of polarization. These walls are either neutral (100) planes or charged (001) planes and (IV) 180° domain walls parallel to the (010) planes and separating domains with opposite sense of both a and c components of polarization. Dark-field TEM image formed using a weak (210) reflection in the [001] zone axis reveals a network of 90° domain walls as shown in Fig. 4. The black and white contrasts in image represent domain variants separated by 90° domain walls. These walls separate domains with their a axis along the $SrTiO_3[110]$ or along the $SrTiO_3[1\bar{1}0]$ directions. The

[a)]Electronic mail: vgopalan@psu.edu

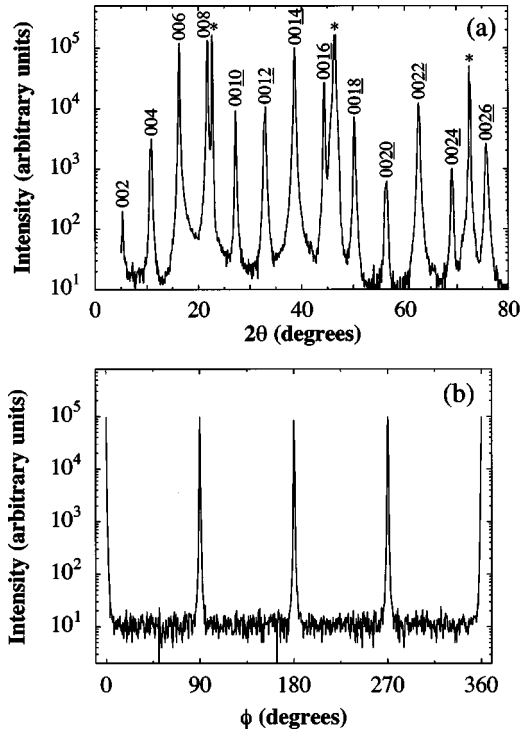

FIG. 1. X-ray diffraction spectra of the $Bi_4Ti_3O_{12}$ thin film deposited on a $SrTiO_3(001)$ substrate using Cu$K\alpha$ wavelength. (a) coupled on axis θ–2θ scan showing that the epitaxial relationship of $Bi_4Ti_3O_{12}(001)$ planes are parallel to the $SrTiO_3(001)$. The rocking curve about the (0016) peak gives a full width at half maximum (FWHM) of 0.3°. The peaks due to the $SrTiO_3$ substrate are marked by asterisks (*). (b) Off axis ϕ-scan of $Bi_4Ti_3O_{12}$ 117 reflections indicating an epitaxial relationship of $Bi_4Ti_3O_{12}[100]//SrTiO_3[110]$ and $Bi_4Ti_3O_{12}[010]//SrTiO_3[\bar{1}10]$. The FWHM of the reflections is ~0.4°. The $\phi=0°$ position is aligned to be parallel to the [100] in-plane direction of the $SrTiO_3$ substrate.

average lateral size of such domains is ~100–200 nm.

Based on the above discussion, we define four classes of domain variants X^+, X^-, Y^+, and Y^- according to whether the *a* component of polarization points in the $SrTiO_3[110]$, $[\bar{1}\bar{1}0]$, $[1\bar{1}0]$, or $[\bar{1}10]$ directions, or alternatively $(+x, -x, +y, -y)$ directions in Fig. 2, respectively. In the following sections, we describe how the X^+, X^-, Y^+, and Y^-

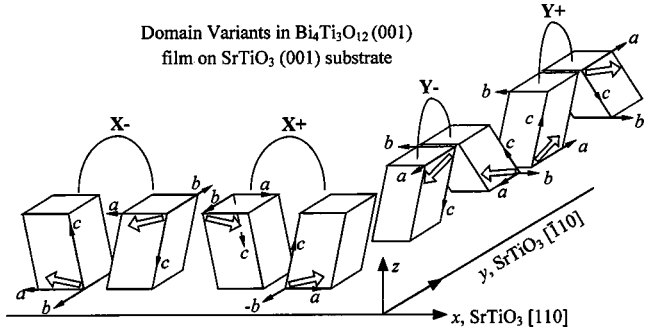

FIG. 2. Schematic description of the eight possible domain configurations of the $Bi_4Ti_3O_{12}$ thin film. Each of the possible domains has a monoclinic unit cell, with lattice parameters $a=5.4500$ Å and $b=5.4059$ Å, $c=32.832$ Å, and $\beta=90.00°$, which slightly deviates from the orthorhombic unit cell. The polarization axis forms an angle of ≈4.5° from the crystallographic *a* axis in the $a-c$ plane as shown by wide arrows. Both the tilt angle β and the angle of polarization from the *a* axis are shown exaggerated in the schematic.

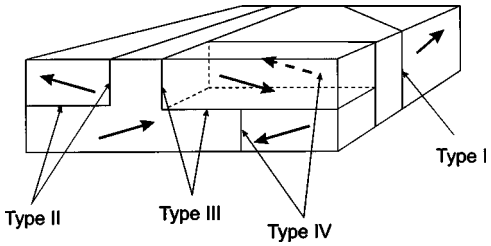

FIG. 3. Schematic illustration of the four different types of domain walls possible in the $Bi_4Ti_3O_{12}$ thin film. (I) Nearly-90° domain walls along the (110) plane. (II) Domain walls separating variants with opposite *a* component of polarization. These walls are either neutral $(001)(a-b)$ planes or charged $(100)(b-c)$ planes. (III) Domain walls separating variants with opposite *c* component of polarization. These walls are either neutral (100) $(b-c)$ planes or charged $(001)(a-b)$ planes. (IV) 180° domain walls parallel to the $(010)(a-c)$ planes and separating domains with opposite sense of both *a*- and *c*- components of polarization. The arrows denote the direction of polarization within each domain.

domains can be distinguished by second harmonic generation measurements in normal incidence to the substrate.

III. SECOND HARMONIC GENERATION MEASUREMENTS

A. Experimental procedure

A schematic description of the experimental setup is shown in Fig. 5. The fundamental beam from a 10 Hz *Q*-switched Nd:YAG laser ($\lambda=1064$ nm) is passed through a series of beam splitters to cut its intensity to approximately 10 mW. The beam is then propagated through a polarizer, half wave plate, focusing lens ($f=500$ mm) and a long-wave pass filter to absorb any residual second harmonic light. The half wave plate is situated on a computer controlled rotating stepper motor to allow the continuous change of the polarization at the input. The sample is placed 50 mm in front of the focal point of the focusing lens, where the beam diameter is approximately 1.2 mm, and the energy density is below the damage threshold. The sample is held with the thin film at the backside of the sample. The output beam is passed

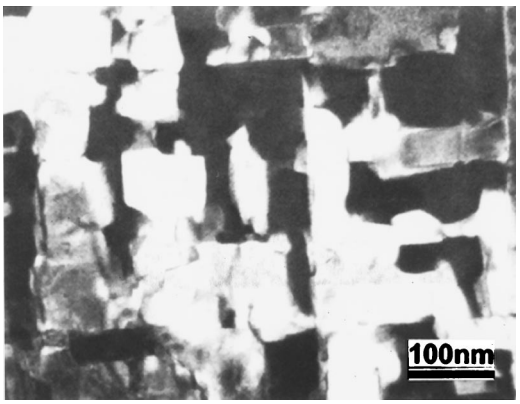

FIG. 4. Network of 90° domain walls as seen in the plan-view dark-field TEM image of a $Bi_4Ti_3O_{12}$ thin film using a weak 210 reflection in the [001] zone axis. These walls run approximately parallel to $SrTiO_3\langle 100\rangle$ directions and separate the bright and dark regions which that correspond to the $X^{+/-}$ and $Y^{+/-}$ domain variants of Fig. 2, respectively. The average lateral size of such domains is ~100–200 nm.

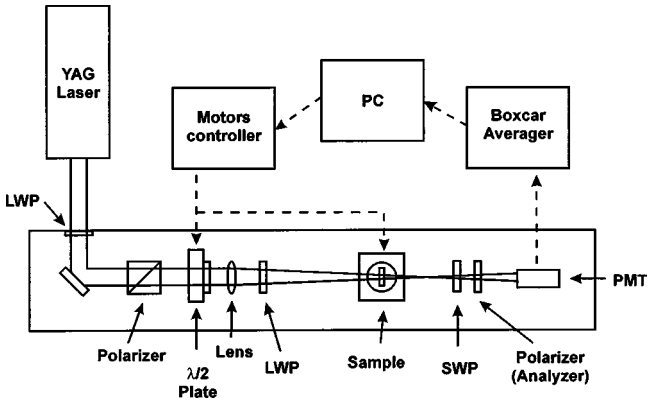

FIG. 5. Schematic description of the experimental setup for SHG measurements.

through a short-wave pass filter to absorb the fundamental light at 1064 nm and the second harmonic signal at 532 nm is analyzed with a polarizer aligned either along the *x* axis ($SrTiO_3[110]$) or *y* axis ($SrTiO_3[1\bar{1}0]$). The beam is then propagated to the photomultiplier tube (PMT) and its intensity is lowered using neutral density filters if needed. The signal from the PMT is fed to a gated integrator and a boxcar averager. The averaged output is read to the computer via an analog-to-digital converter.

The measurement starts with the light polarization parallel to the $Bi_4Ti_3O_{12}$ thin film [010] and with the analyzer either parallel or perpendicular to that direction. (The $SrTiO_3$ substrate is cubic, and it was confirmed that it does not result in any second harmonic response.) The incident polarization is changed by rotating the half-wave plate while keeping the analyzer fixed. The measurement is made once with the analyzer along the *x* axis and once along the *y* axis. A typical polar–plot pair of the SHG intensity as a function of input polarization angle for the two different output polarizations of the 532 nm light is shown in Fig. 6. The experimental data is shown as circles, while the solid line is a fit obtained from the theoretical model described as follows. These plots provide information on the specific distribution of domains in the area probed. In general, a different area on the film gives slightly different polar plots, however, all these plots can be analyzed within the theoretical framework described in the following section.

B. Theoretical model

In order to describe the expected SHG intensity from the thin film ($I^{2\omega}$), the net polarization at the second harmonic frequency ($P^{2\omega}$), should be calculated along a global coordinate system (*x*, *y*, *z*) of the substrate (shown in the schematic of Fig. 2). Referring first to the monoclinic unit cell coordinates (*a*, *b*, and *c*) of $Bi_4Ti_3O_{12}$, the second harmonic polarization components are given by

$$\begin{bmatrix} P_a \\ P_b \\ P_c \end{bmatrix}^{(2\omega)} = \begin{pmatrix} d_{11} & d_{12} & d_{13} & 0 & d_{15} & 0 \\ 0 & 0 & 0 & d_{24} & 0 & d_{26} \\ d_{31} & d_{32} & d_{33} & 0 & d_{35} & 0 \end{pmatrix} \times \begin{pmatrix} E_a^2 \\ E_b^2 \\ E_c^2 \\ 2E_bE_c \\ 2E_cE_a \\ 2E_aE_b \end{pmatrix}^{(\omega)} . \quad (1)$$

Here, the electric fields E_a, E_b, and E_c are the electric fields of the incident light at the optical frequency ω inside the thin film and d_{ij} are the nonlinear coefficients, where the subscripts $i,j=(1,2,\text{and}\,3)$ correspond, respectively, to the coordinates (*a*, *b*, and *c*) of the unit cell. The superscripts (ω) and (2ω) are simply labels referring to the frequency of the incident electric fields, E^{ω}, and the nonlinear polarizations $P^{2\omega}$.

We assume the fundamental wave is a plane-wave propagating along the *z* direction and incident normal to the film. This assumption has been found to be quite good when comparing the predicted nonlinear coefficients from the model with known nonlinear coefficients of reference samples.[6] This, we believe, is due to the fact that the incident gaussian beam is very weakly focused (beam divergence ~0.01 rad), and the sample is placed close to the focal point where the beam incident on the sample is large (1.2 mm). Further, due to the large index, *n*, of the film, any external

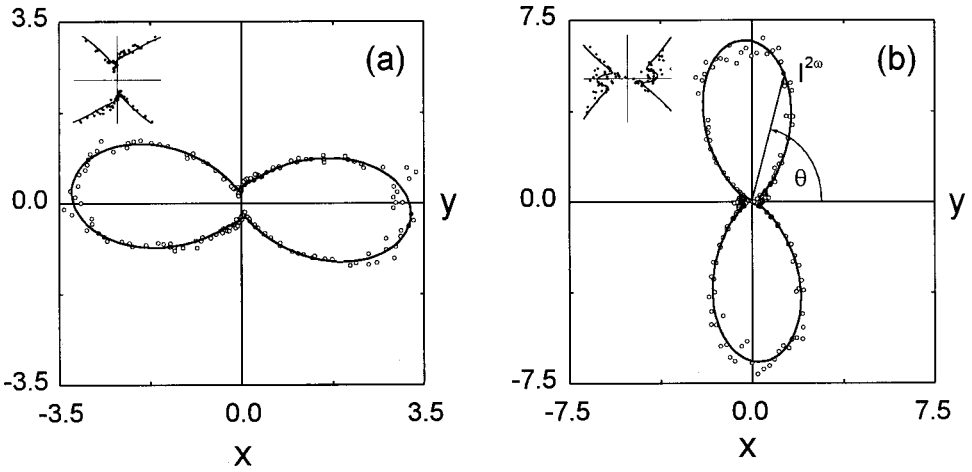

FIG. 6. Polar plots of the SHG intensity $I^{2\omega}(\lambda=532\,\text{nm})$ as a function of input polarization angle, $\theta(\lambda=1064\,\text{nm})$ for the output polarization of the SHG light along (a) $SrTiO_3[\bar{1}10]$ (*y* axis), and (b) $SrTiO_3[110]$ (*x* axis). The experimental data is shown as circles, while the solid line is a fit obtained based on Eq. (5) derived from the theoretical model presented in the article. Inset shows the details around the origin.

TABLE I. Nonlinear polarization for the four variants shown schematically in Fig. 2.

Variant	P_x(analyzer $\parallel x$)	P_y(analyzer $\parallel y$)
X^+	$\frac{1}{\sqrt{2}}(d_{11}\sin^2\theta+d_{12}\cos^2\theta)(E^\omega)^2$	$\frac{1}{\sqrt{2}}d_{26}\sin 2\theta(E^\omega)^2$
X^-	$-P_x^{X+}$	$-P_y^{y+}$
Y^+	$\frac{1}{\sqrt{2}}d_{26}\sin 2\theta(E^\omega)^2$	$\frac{1}{\sqrt{2}}(d_{11}\cos^2\theta+d_{12}\sin^2\theta)(E^\omega)^2$
Y^-	$-P_x^{Y+}$	$-P_y^{Y+}$

beam divergence is further reduced by approximately a factor of ~2.7–2.8 upon entering the film. These conditions therefore justify the plane-wave approximation. The incident electric field E^ω has a polarization rotating in the $x-y$ plane, forming an angle θ with the y axis, the incident electric fields along x and y axes are $E_x^\omega = E^\omega \sin\theta$ and $E_y^\omega = E^\omega \cos\theta$. During the measurement, the output analyzer is fixed either along the x or y axis. For normal incidence, as in our case, $E_z = 0$ and, therefore, contributions to the SHG field are only due to d_{11}, d_{12}, and d_{26}. Following the theoretical derivation outlined in a previous publication,[6] the nonlinear polarizations created in the four classes of domain variants can be calculated as a function of E^ω and θ as shown in Table I. These nonlinear polarizations now radiate light at a frequency of 2ω, with intensity $I^{2\omega} \propto P^{2\omega}(P^{2\omega})^*$, where the $*$ superscript represents the complex conjugate of the nonlinear polarization. Note that the nonlinear polarizations of the domain variants X^+ and X^- are identical in magnitude, but differ by a minus sign indicating a phase difference of π or 180°. The same is true for nonlinear polarizations of domain variants Y^+ and Y^-. The relative phase shift of π between two domain variants results in a net destructive interference of the second harmonic signal since the film thickness is much smaller than coherence length. (In the special case of quasiphase matched second harmonic generation, the presence of periodic 180° domains creates a π phase shift in the second harmonic signal *every coherence length*, which enhances the overall harmonic generation efficiency. However in the present case, for π phase shifts at distances shorter than the coherence length, the result is destructive interference).

Referring to the domain microstructure in $Bi_4Ti_3O_{12}$ (see Fig. 3), the X^+ and an X^- domain variants are separated by type II domain walls which are either neutral (001) planes or charged (100) planes, where the plane indices refer to the pseudo-orthorhombic unit cell of $Bi_4Ti_3O_{12}$. The $a-b$ domain walls will run parallel to the growth interface [$SrTiO_3$(001)], and, therefore, give rise to domain patterns in the cross sectional thickness of the film. The film thickness studied here is $t \sim 0.1\,\mu$m. This is lower than the coherence length $l_c = \lambda/2(n^{2\omega} - n^\omega)$ for phase matched second harmonic generation in the film. Using bulk index dispersion relations[7] of $Bi_4Ti_3O_{12}$ crystals, we estimate the coherence lengths for a axis polarized fundamental light at 1064 nm to be $l_c \sim 3.36\,\mu$m, and for b-polarized light, $l_c \sim 2.89\,\mu$m. Consider light passing through the film thickness in an area dA^X. It passes through a *thickness fraction* t^{X^+} of the X^+ domain and t^{X^-} of the X^- domain, making the net nonlinear polarization generated by the combination of the two domain variants proportional to $(t^{X^+} - t^{X^-})(P^{X^+})^{2\omega}$. This relationship reflects the net destructive interference of the second harmonic electric fields created by each domain variant due to the π phase shift between the two fields. Therefore, the combined second harmonic response from the X^+ and X^- domains arises from only a net difference in their abundance. If A^X represents the total area fraction of the probed film area composed of X^+ and X^- domains, then the net nonlinear polarization along x or y polarized light from this area is given by

$$P_{x,y}^X = \left(\int_0^{A^X} (t^{X^+} - t^{X^-})\, dA^X \right) P_{x,y}^{X^+}, \tag{2}$$

where the superscript 2ω has been dropped for convenience, and the nonlinear polarizations are henceforth understood to be at this frequency. The integral expression inside the bracket in Eq. (2) is defined as ΔA_x. In words, ΔA_x is the *net* thickness fraction of X^+ domains with respect to X^- domains, i.e., the relative thickness fraction of domains with the a component of their polarization along $SrTiO_3$ [110] versus $[\bar{1}10]$ directions. This expression also implicitly includes areas of exclusive X^+ (with $t^{X^+} = 1$) and X^- (with $t^{X^-} = 1$) domains, which are separated by charged domain walls of type II perpendicular to the substrate plane, or are spatially separated by Y^+ and Y^- domains though 90° domains walls of Type I. This analysis, therefore, assumes *complete phase correlation*, which implies that the second harmonic response of all domain variants are phase correlated. This assumption is justified in our present case since the domain sizes of X^+ and X^- variants are of the order of 100–200 nm in the film growth plane, which is less than the wavelength of light (see Fig. 4). Using similar arguments, we can also write the net nonlinear response from Y^+ and Y^- domains as

$$P_{x,y}^Y = \left(\int_0^{A^Y} (t^{Y^+} - t^{Y^-})\, dA^Y \right) P_{x,y}^{Y^+}, \tag{3}$$

where A^Y represents the total area fraction of the probed film area composed of Y^+ and Y^- domains. The integral expression inside the bracket in Eq. (3) is defined as ΔA_y, which is the *net* thickness fraction of Y^+ domains with respect to Y^- domains, i.e., the relative thickness fraction of domains with the a component of their polarization along $SrTiO_3$ $[1\bar{1}0]$ versus $[\bar{1}10]$ directions. The total nonlinear polarization from the film can now be written as

$$P_{x,y} = \Delta A_x P_{x,y}^X + \Delta A_y P_{x,y}^Y e^{i\Gamma}. \tag{4}$$

The phase shift Γ is the difference in phase of the nonlinear polarizations arising from $X^{(+/-)}$ and $Y^{(+/-)}$ domains, and is given by $\Gamma = 2\omega/c(n_b^{2\omega} - n_a^{2\omega}).t$, where n_b and n_a are the refractive indices of $Bi_4Ti_3O_{12}$ at the SHG frequency, along the crystallographic b and a axes, respectively, and t is the film thickness. The second harmonic intensity from the film, $I^{2\omega} \propto P^{2\omega}.(P^{2\omega})^*$, can now be calculated:

$$I_j^{2\omega} = K_{1,j}(\sin^2\theta + K_{2,j}\cos^2\theta)^2 + K_{3,j}\sin^2 2\theta + K_{4,j}(\sin^2\theta + K_{2,j}\cos^2\theta)\sin 2\theta, \tag{5}$$

where $j=x$ or y denotes the polarization direction, and K_{ij} are the phenomenological fitting parameters. Using Table I, we can show the following relations between these parameters and the physical quantities:

$$\frac{d_{12}}{d_{11}}=K_{2,x}=(K_{2,y})^{-1}, \tag{6}$$

$$\left(\frac{d_{26}}{d_{12}}\right)^4=\left(\frac{K_{3,x}}{K_{1,x}(K_{2,x})^2}\right)\left(\frac{K_{3,y}}{K_{K_{1,y}}}\right), \tag{7}$$

$$\left(\frac{d_{26}}{d_{11}}\right)^4=\left(\frac{K_{3,y}}{K_{1,y}(K_{2,y})^2}\right)\left(\frac{K_{3,x}}{K_{1,x}}\right), \tag{8}$$

$$\cos^2\Gamma=\frac{(K_{4,x})^2}{4K_{1,x}K_{3,x}}=\frac{(K_{4,y})^2}{4K_{1,y}K_{3,y}}, \text{ and} \tag{9}$$

$$\left(\frac{\Delta A_x}{\Delta A_y}\right)^4=\left(\frac{K_{3,y}}{K_{1,y}(K_{2,y})^2}\right)\left(\frac{K_{1,x}}{K_{3,x}}\right). \tag{10}$$

The fitting coefficients K_{ij} can be determined from the experimental measurements. Equations (6) and (8) can be used to determine two independent ratios; d_{12}/d_{11} and d_{26}/d_{11}. Equation (7) then provides a consistency check for the ratio d_{26}/d_{12}. The phase shift Γ can be determined from Eq. (9), which in turn can be used to determine the material birefringence $\Delta n=(n_b^{2\omega}-n_a^{2\omega})$. Note that the parameters d_{12}/d_{11}, d_{26}/d_{11}, and Δn are *intrinsic* material properties, and can be determined *independent* of the domain microstructure, i.e., the relative area fractions of the eight different types of domain variants. Equation (10) provides new *microstructural* information, $\Delta A_x/\Delta A_y$, in the area probed.

IV. RESULTS AND DISCUSSION

In Fig. 6, the theoretical model for the second harmonic signal intensity ($I_x^{2\omega}$ and $I_y^{2\omega}$), derived in Eq. (5), is fitted (solid line) to the experimental data (circles) by using nonlinear least-square fitting. The fitting of experimental polar plots is facilitated by the following guidelines: the first term in Eq. (5) gives rise to a two-lobed structure, while the second term to a four-lobed structure. The third term, is a cross term which produces a phase shift, causing a rotation of the lobes. Thus K_1 increases the strength of the two-lobed structure, and K_3 of the four-lobed structure. The phase shift depends on K_4 and the constant K_2 is the ratio of the magnitude of the intensity along the y axis ($\theta=0$) to that along the x axis ($\theta=90°$). Since K_2 is related only to the d_{ij} coefficients, this ratio is a pure material property, independent of the domain statistics. Since K_1 and K_3 are related to ΔA_x and ΔA_y, as the ratio of $\Delta A_x/\Delta A_y$ increases, the polar plot becomes increasingly two-lobed for output polarization along the x axis and increasingly four lobed for output polarization along the y axis.

From the phenomenological fitting parameters to these measurements, the following ratios were calculated for the nonlinear coefficients: $d_{12}/d_{11}=-3.498\pm0.171$, $|d_{26}/d_{12}|=0.365\pm0.010$, and $|d_{26}/d_{11}|=1.273\pm0.036$. Note that from Eq. (6), we have also determined without ambiguity, that the *signs* of d_{12} and d_{11} are opposite, as indicated by the negative sign of the ratio d_{12}/d_{11}. The linear birefringence was determined to be: $|\Delta n^{2\omega}|=0.101\pm0.018$, and the ratio of the net area fraction was calculated to be: $\Delta A_x/\Delta A_y=0.833\pm0.024$. Assuming equal probability of all domain variants, this ratio would on the average be expected to be equal to 1. However, in probing the local area of $\sim 0.36\pi$ mm^2, one sensitively detects the local deviation of the $\Delta A_x/\Delta A_y$ from 1. On moving the beam to different locations, the shapes of the polar plots change, and the corresponding $\Delta A_x/\Delta A_y$ ratio changes as well, varying by $\pm 15\%$–20% about the value of 1.

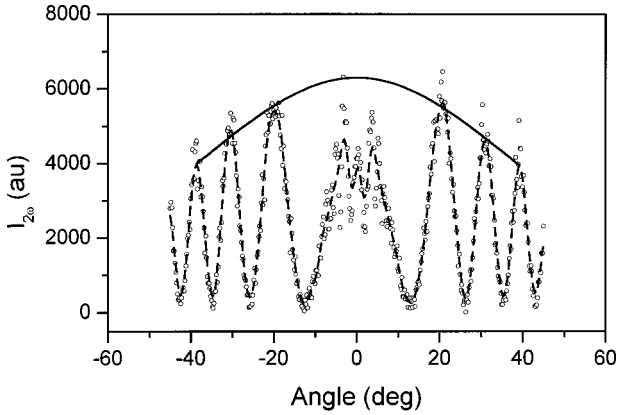

FIG. 7. Maker fringes pattern of the SHG light intensity ($\lambda=532$ nm) as a function of incidence angle (from surface normal) of fundamental light ($\lambda=1064$ nm) for a z-cut single domain $LiTaO_3$ crystal in transmission geometry. Both the incident light and the SHG light were TE polarized along the crystallographic y axis of the crystal, thus probing the nonlinear coefficient d_{22}. The circles represent the experimental data points. The dashed line is the approximation to the fringes, obtained using nonlinear Fourier smoothing. The Maker peaks location and intensities are used to obtain the Lorentzian envelope (solid line). The value of the Lorentzian peak (bold solid line) at normal incidence is used as a reference to calculate the absolute values of area fractions ΔA_x and ΔA_y in $Bi_4Ti_3O_{12}$ thin films (See Eqs. (3) and (4) for definitions).

To the best of our knowledge, the nonlinear d_{ij} coefficients for single crystal $Bi_4Ti_3O_{12}$ have not been reported in the literature before. However, the optical birefringence $\Delta n^{2\omega}=(n_b^{2\omega}-n_a^{2\omega})$ has been reported in the literature for $Bi_2Ti_3O_{12}$ single crystals as $\Delta n^{2\omega}\sim 0.111\pm0.035$, which agrees well with our calculated value.[8]

Knowledge of at least one nonlinear coefficient out of d_{26}, d_{11}, and d_{12} can yield the other two coefficients, using the aforementioned relations given. The absolute values of ΔA_x and ΔA_y can also be found by performing SHG intensity reference measurements on a well known crystal. The reference crystal used here was a z-cut single crystal single domain $LiTaO_3$ crystal, 0.52 mm thick for which $d_{22}=4.4\,d_{36}(KH_2PO_4)=1.6720$ pm/V.[9,10] The Maker fringes[11] were measured for this crystal by measuring the intensity of the second harmonic intensity as a function of incidence angle for a transverse electric (TE) polarized incident light. The Maker fringes measurement is shown in Fig. 7. The reference intensity value was calculated using the nonlinear coefficient d_{22} and the maximum intensity of the envelope of fringes at normal incidence. Following the derivation given in Ref. 12, we then find the nonlinear coefficient of the film in a specific geometry as:

$$d_f^2 = d_r^2 \frac{P_f^{2\omega}}{P_r^{2\omega}} \frac{n_f^{2\omega}}{n_r^{2\omega}} \left(\frac{n_f^{\omega}}{n_r^{\omega}}\right)^2 \left(\frac{l_{c,f}}{l_{c,r}}\right)^2 \frac{\sin^2\left(\frac{\pi l_r}{l_{c,r}}\right)}{\sin^2\left(\frac{\pi l_f}{l_{c,f}}\right)} \left(\frac{T_f^{\omega}}{T_r^{\omega}}\right)^4. \quad (11)$$

Here, the indices f and r represent the film and reference respectively, $P^{2\omega}$ is the measured SHG intensity, $n^{2\omega}$ and n^{ω} represent the indices of refraction at the SHG wavelength and at the fundamental wavelength, respectively, l_f and l_r are the thickness of film and reference crystal, respectively, l_c is the coherence length and T is the transmittance given by $T^{\omega} \propto 1/(1+n^{\omega})$. Referring to Eq. (5), the intensity of the SHG from the film at an incidence angle of $\theta = 0°$ yields $I_x^{2\omega}(\theta = 0°) \propto (\Delta A_x d_{12})^2$ and $I_y^{2\omega}(\theta = 0°) \propto (\Delta A_y d_{11})^2$. Similarly, $I_x^{2\omega}(\theta = 90°) \propto (\Delta A_x d_{11})^2$ and $I_y^{2\omega}(\theta = 90°) \propto (\Delta A_y d_{12})^2$. On comparison with the reference signal according to Eq. (11), and assuming bulk refractive indices from Ref. 7, we can determine $(\Delta A_x d_{11})^2 = 5.15 \times 10^{-3}\,(\mathrm{pm/V})^2$ and $(\Delta A_y d_{11})^2 = 7.46 \times 10^{-3}\,(\mathrm{pm/V})^2$. However, the absolute values of ΔA_x and ΔA_y can only be determined from the knowledge of at least one of the coefficients d_{11}, d_{12}, and d_{26}, which are currently undetermined.

V. CONCLUSIONS

This work has presented second harmonic generation measurements along with theoretical modeling of the response from a composite domain microstructure in a $Bi_4Ti_3O_{12}$ thin film on a $SrTiO_3$ substrate. The treatment yields quantitative information on basic material properties, such as the ratios of nonlinear optical coefficients, and optical birefringence, as well as microstructural information specific to the area probed, such as relative fractions of different domain variants in the film. The following nonlinear coefficients and birefringence were determined: $d_{12}/d_{11} = -3.498 \pm 0.171$, $|d_{26}/d_{12}| = 0.365 \pm 0.010$, $|d_{26}/d_{11}| = 1.273 \pm 0.036$, and $|n_b - n_a| = 0.101 \pm 0.018$ (at 532 nm). The relative thickness fractions $\Delta A_x/\Delta A_y$, representing the ratio of the *net* fraction of *a* component of polarization in the *x* to that in *y* directions could be determined sensitively in the probed area (see Eqs. (2) and (3) for definitions).

The technique of SHG measurements presented here to probe materials structure is quite general. Since the property is a third rank tensor, it is very sensitive to the point group symmetry of the material. In particular, it arises from a lack of center of inversion symmetry, and therefore surfaces, interfaces, and materials with point groups without inversion symmetry would give rise to second harmonic response. Under nonphase matched conditions, the technique probes material surfaces down to a depth of approximately the coherence length. Films which are thinner than coherence length, l_c (typically $l_c \sim$ micrometers in ferroelectrics) can therefore be studied without phase matching considerations. A simple theoretical analysis of the information is possible in this case with the knowledge of all the possible structural variants and wall configurations that separate them. We are currently employing this technique to probe dynamic changes in the domain microstructure that occur under external electric fields and by varying the temperature.

ACKNOWLEDGMENT

This work was supported by the National Science Foundation CAREER award (No. 9984691).

[1] C. A. Paz de Araujo, J. D. Cuchiaro, L. D. McMillan, M. C. Scott, and J. F. Scott, Nature (London) **374**, 627 (1995).
[2] R. E. Newnham, R. W. Wolfe, and J. F. Dorrian, Mater. Res. Bull. **6**, 1029 (1971).
[3] S. E. Cummins and L. E. Cross, J. Appl. Phys. **39**, 2268 (1968).
[4] C. D. Theis, J. Yeh, D. G. Schlom, M. E. Hawley, G. W. Brown, J. C. Jiang, and X. Q. Pan, Appl. Phys. Lett. **72**, 2817 (1998).
[5] A. D. Rae, J. G. Thompson, R. L. Withers, and A. C. Willis, Acta Crystallogr., Sect. B: Struct. Sci. **46**, 474 (1990).
[6] V. Gopalan and R. Raj, J. Am. Ceram. Soc. **79**, 3289 (1996).
[7] W. L. Bond, J. Appl. Phys. **36**, 1674 (1965).
[8] M. Simon, F. Mersch, C. Kuper, S. Mendricks, S. Wevering, J. Imbrock, and E. Kratzig, Phys. Status Solidi A **159**, 559 (1997).
[9] Landolt–Börenstein, *Numerical Data and Functional Relationships in Science and Technology*, New Series, Group III, Vol. 12, edited by K. H.-Hellwege and A. M. Hellwege (Springer, Berlin, 1978).
[10] R. C. Eckardt, H. Masuda, Y. X. Fan, and R. L. Byer, IEEE J. Quantum Electron. **26**, 922 (1990).
[11] P. D. Maker, R. W. Terhune, M. Nisenoff, and C. M. Savage, Phys. Rev. Lett. **8**, 21 (1962).
[12] A. Yariv, *Quantum Electronics* (Wiley, New York, 1989).